

REVIEW**The Main Sequence of quasars: the taming of the extremes[†]**

P. Marziani^{*1} | E. Bon² | N. Bon² | M. D’Onofrio³ | B. Punsly⁴ | M. Śniegowska⁵ | B. Czerny^{5,6} | S. Panda^{6,5} | M. L. Martínez Aldama⁶ | A. del Olmo⁷ | A. Deconto-Machado⁷ | C. A. Negrete⁸ | D. Dultzin⁸ | T. Buendia⁸ | K. Garnica⁸

¹Padua Astronomical Observatory, National Institute for Astrophysics (INAF), Padua, Country name

²Astronomical Observatory, Belgrade, Serbia

³Department of Physics and Astronomy “Galileo Galilei”, University of Padua, Padua, Italy

⁴ICRA, Physics Department, University La Sapienza, Rome, Italy

⁵Nicolaus Copernicus Astronomical Center, Polish Academy of Sciences, Warsaw, Poland

⁶Center for Theoretical Physics, Polish Academy of Sciences, Warsaw, Poland

⁷Instituto de Astrofísica de Andalucía, CSIC, Granada, Spain

⁸Instituto de Astronomía, UNAM, Mexico, Mexico

Correspondence

*Paola Marziani Email: paola.marziani@inaf.it

The last few years have seen the confirmation of several trends associated with the quasar main sequence. The idea of a main sequence for quasars is relatively recent, and its full potential for the observational classification and contextualization of quasars’ properties has yet to be fully exploited. The main sequence drivers are discussed in terms of the properties of extreme objects. We briefly summarize developments that constrain the viewing angle of the accretion disk in a particular class of quasars (extreme Population B, radiating at low Eddington ratio), as well as inferences on the chemical composition of the broad line emitting gas, and on the nature of radio emission along the quasar main sequence.

KEYWORDS:

galaxies: active — quasars: general — quasars: emission lines — galaxies: starburst — radio continuum: galaxies

1 | INTRODUCTION: A MAIN SEQUENCE FOR TYPE-1 (UNOBSURED) QUASARS

The main sequence (MS) concept originated from a Principal Component Analysis on the spectra of Palomar Green quasars that allowed the identification of a first Eigenvector (Eigenvector 1, E1). The E1 was found to be associated with an anti-correlation between strength of the singly ionized iron emission blend centered at λ 4570 (FeII λ 4570) and the FWHM of H β (or peak intensity of [OIII] 4959,5007). The MS itself can be effectively represented in a plane where the FWHM H β data are diagrammed against the parameter R_{FeII} defined as the

flux ratio between FeII λ 4570 and the broad component of H β i.e., $R_{\text{FeII}} = F(\text{FeII}\lambda 4570)/F(\text{H}\beta_{\text{BC}})$. Figure 1 shows a sketch of the occupation of the quasar MS in this parameter plane.

The MS has withstood the test of time; from the original 80 sources in the paper by Boroson & Green (1992) and the tens of objects in an even earlier study by Gaskell (1985), the MS has been detected and studied in sample of ~ 200 objects (Sulentic et al., 2002), ~ 500 (Zamfir, Sulentic, Marziani, & Dultzin, 2010), to ~ 20000 (Shen & Ho, 2014). The main trends have been confirmed, extended to multifrequency data related to the accretion process and the accompanying outflows (Sulentic, Marziani, & Dultzin-Hacyan 2000; Sulentic, Marziani, Zwitter, Dultzin-Hacyan, & Calvani 2000, see also the summary Table of Fraix-Burnet, Marziani, D’Onofrio, & Dultzin 2017), and revealed also by sophisticated techniques such as locally linear embedding in manifold learning (Jankov, Ilić, & Kovačević, 2021).

[†]Invited talk presented at the XIII Serbian Meeting on spectral line shapes in astrophysics (SCSLSA)

⁰**Abbreviations:** AGN: active galactic nuclei; BLR: broad line region; E1: Eigenvector 1; FWHM: full width half maximum; MS: main sequence; NLSy1: narrow-line Seyfert 1; Pop. A: Population A; Pop. B: Population B; RL: radio loud; RQ: radio quiet; SED: spectral energy distribution; xA: extreme Population A

Why are the seemingly-obscure parameters FWHM $H\beta$ and R_{FeII} so revealing? FeII emission is self-similar in type-1 AGN but the relative flux to $H\beta$ (parameterized by R_{FeII}) can vary from undetectability to $R_{\text{FeII}} \gtrsim 2$, with values larger than ≈ 2 being exceedingly rare. The FeII emission extends from UV to the IR and can dominate the thermal balance of the low-ionization broad-line region (BLR; Marinello, Rodriguez-Ardila, Garcia-Rissmann, Sigut, & Pradhan, 2016). The FWHM of $H\beta^1$ is related to the velocity field in the low-ionization part of the BLR (predominantly virialized) and to viewing angle effects. Therefore these two parameters reflect important aspects of the emitting gas physical conditions and dynamical status, along with the orientation (defined as the angle θ between a putative axis of symmetry and the line of sight at which the AGN is seen). The MS includes only type-1 AGN i.e., sources for which broad lines are visible in natural light. According to the unification schemes, θ is constrained between 0 and $\sim 45 - 60$ degrees (Antonucci, 1993; Urry & Padovani, 1995, see also Marin 2016 for a more recent perspective). Effects of changing θ on the line width are believed to be significant for radio-quiet type-1 AGN as well, although there is not as yet an established view to connect θ to observed spectral parameters. Orientation definitely plays a role in beamed radio emission (Urry & Padovani, 1995), although the effects on the broad optical and UV lines are subject of current debate (more in § 3.2).

The elbow-shaped MS allows for the definition of two main populations: Population A and B (Sulentic, Marziani, & Dultzin-Hacyan, 2000, hereafter Pop. A and Pop. B respectively) on the basis of a limit on the FWHM of $H\beta$ ($\approx 4000 \text{ km s}^{-1}$ at low and moderate luminosity), as well as of several spectral types in narrow ranges of FWHM and R_{FeII} . The Population A and B spectra are usually so very different that their classification can be recognized by eye: Pop. A sources show sharp $H\beta$ profiles, prominent FeII, and weak $[\text{OIII}]\lambda\lambda 4959, 5007$ emission; on the converse a typical Pop. B spectrum shows Gaussian-line $H\beta$ profiles, weak FeII, and strong and spiky $[\text{OIII}]$ (see the Figures in Sulentic, Marziani, & Dultzin-Hacyan 2000). If one compares a high-ionization line such as $\text{CIV}\lambda 1549$ to $H\beta$, the first shows a significant shift to the blue with respect to the quasar rest frame.² Summing up decades of works in monitoring and in the study of the spectroscopic properties of quasars, we can say that the emitting region can be heuristically subdivided in two sub-regions: a low ionization, closely associated with the accretion disk, and that has been found to be predominantly in virial dynamical equilibrium, for both Pop. A and B (even with significant differences that are still poorly understood), and an outflow/wind

region (Collin-Souffrin, Dyson, McDowell, & Perry, 1988; Elvis, 2000), by far more evident in Pop. A and especially in extreme Population A (xA, defined by $R_{\text{FeII}} > 1$; see Fig. 1). The aim of this paper is to emphasize the danger of ignoring the trends of the main sequence, by showing how different the objects at the opposite extreme ends are.

Before discussing the interpretation of the main sequence (Section 2), it is helpful to consider why there is a special reason to prefer 4000 km s^{-1} , instead of 2000 km s^{-1} for the $H\beta$ FWHM limit. Most studies still distinguish narrow-line Seyfert 1 (NLSy1s, defined from the condition $\text{FWHM } H\beta \lesssim 2000 \text{ km s}^{-1}$) as a distinct class, and compare NLSy1s to “broad-line” AGN. However, the $H\beta$ profiles remain Lorentzian-like up to around $\text{FWHM}(H\beta) = 4000 \text{ km s}^{-1}$, and the $\text{CIV}\lambda 1549$ blueshifts remain consistent up to around the same FWHM limit (Marziani, del Olmo, et al., 2018). A clear change in the $H\beta$ line profiles occurs at $\text{FWHM}(H\beta) \approx 4000 \text{ km s}^{-1}$: composite profiles in the range $3000 \text{ km s}^{-1} \lesssim \text{FWHM}(H\beta) \lesssim 4000 \text{ km s}^{-1}$ are best fit with a Lorentzian function, while for $4000 \text{ km s}^{-1} \lesssim \text{FWHM}(H\beta) \lesssim 5000 \text{ km s}^{-1}$ a double Gaussian provides a best fit (Sulentic et al., 2002).

The overview of the MS interpretation (Section 2) is followed by an analysis of chemical composition and orientation effects among Pop. B sources (Section 3). The results on chemical compositions are mirrored by the ones obtained for Pop. A (Section 4). In the case of xA, a novel result summarized in §4.2 is the connection between the defining property of strong FeII emission and significant radio power, that mirrors the “jetted” origin of the tremendous radio power of some 20 % of Pop. B sources (Zamfir, Sulentic, & Marziani, 2008). Our conclusion (Section 5) stresses how the improvement in our understanding of quasar physics might be instrumental in the use of xA quasars as cosmological probes.

2 | INTERPRETATION OF THE MAIN SEQUENCE

Several approaches consistently support a relation between L/L_{Edd} and R_{FeII} . For example, the average of the stellar velocity dispersion of the host galaxy in narrow luminosity bins (a proxy for M_{BH}) decreases with R_{FeII} implying that L/L_{Edd} increases with R_{FeII} (Sun & Shen, 2015). The L/L_{Edd} computed from the virial black hole mass M_{BH} relation for sources with reverberation mapping data is correlated with R_{FeII} (Du et al., 2016).

A toy model that assumes a virial relation for M_{BH} in the form:

$$M_{\text{BH}} = f(\theta) \frac{r_{\text{BLR}} \text{FWHM}^2}{G} \quad (1)$$

where $f(\theta)$ is the viewing-angle dependent virial factor shows that the occupation of the MS optical plane at low- z can

¹For the sake of simplicity we shall omit the subscript BC from now on.

²Most precisely traced by low-ionisation narrow emission lines such as $[\text{OII}]\lambda 3727$ (N. Bon et al., 2020).

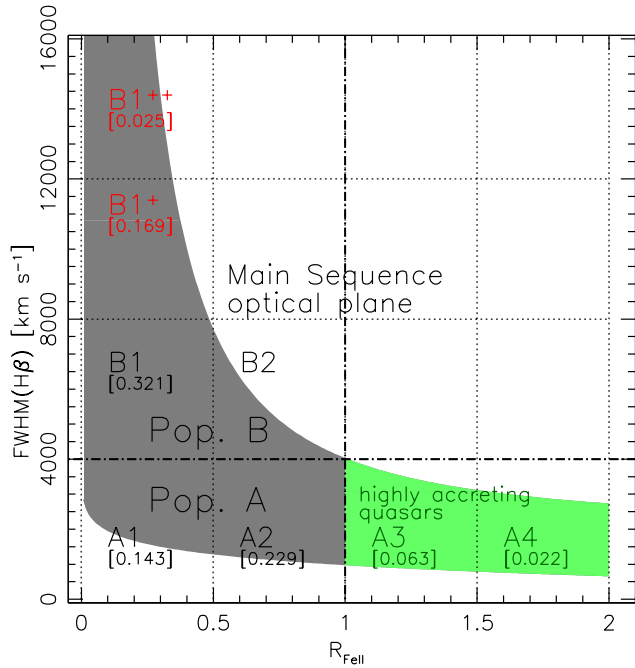


FIGURE 1 A sketch representing the occupation of MS quasars in the plane $\text{FWHM H}\beta$ vs R_{FeII} , the MS “optical plane.” Each bin in the plane corresponds to a spectral type. The ones associated with extreme Pop. B (red labels, top left) and the xA of highly-accreting quasars at the high end of the R_{FeII} distribution satisfying the condition $R_{\text{FeII}} \geq 1$ (green area) are the ones considered in this paper. The numbers in square brackets below each spectral type designation are the source fractional occupation in an optically-selected sample (Marziani et al., 2013).

be accounted for in terms of Eddington ratio and orientation (Marziani, Sulentic, Zwitter, Dultzin-Hacyan, & Calvani, 2001).

Figure 2 shows the prediction of the toy model overlaid to the shape representing the occupation of the AGN in the optical plane of the MS. A surprising aspect of the MS is that the sources radiating at higher L/L_{Edd} are also the ones showing a spectrum of lower ionization degree. Here we just recall that the basis of the toy model (developed in Marziani et al. 2001, and expanded in Panda, Marziani, & Czerny 2019, where a systematic analysis is presented; see also Marziani, Dultzin, et al. 2018 for a summary description) is the connection between ionization parameter and FeII prominence that requires a systematic change in gas density and other physical parameters such as metallicity Z . Orientation effects are then compounded assuming a virial velocity field in a flattened configuration, and possible limb darkening effects on the FeII emission. Not only L/L_{Edd} is roughly proportional to R_{FeII} , but also the elbow

shape of the MS is accounted for by the combination of orientation and L/L_{Edd} variation (Fig. 2). Orientation yields an almost vertical (i.e., parallel to the FWHM axis) displacement from broader to narrower profiles, passing from viewing angle $\theta \approx 50$ to $\theta \approx 5$. Population B sources (broader, with $R_{\text{FeII}} \lesssim 0.5$) are associated with low Eddington ratio ($L/L_{\text{Edd}} \lesssim 0.25$), while Pop. A sources are mostly associated with higher Eddington ratio. Extreme Pop. B means that Eddington ratio can be as low as $L/L_{\text{Edd}} \lesssim 0.01$, with by definition very broad, but also often double-peaked or irregular Balmer line profiles (Ganci et al., 2019). On the converse, xA means sources that are radiating at maximum luminosity-to-black hole mass, at high (possibly super-Eddington) accretion rates (Marziani et al., 2014, see also D’Onofrio, Marziani, & Chiosi 2021 for a recent review).³

An interesting inference from the grid shape is that some Pop. B might appear as Pop. A because of the effect of orientation, since the observed $\text{FWHM} \propto \delta v_K \cdot \sin \theta$ where the v_K is the intrinsic Keplerian velocity field. For $\theta \rightarrow 0$, the FWHM might become $\text{FWHM H}\beta \lesssim 4000 \text{ km s}^{-1}$. These sources are however expected to be rare, since the probability of observing a source at angle θ is also $P(\theta) \propto \sin \theta$. Intrinsic variability may move the sources across the main sequence. As we progress towards the B1⁺⁺, the variability amplitude becomes larger, and we may have variations of FWHM as well for the same object and therefore same mass and inclination, so we have even larger areas on this plot that an object could take. A case study is provided by the extensively-monitored Pop. B source NGC 5548 (N. Bon, Bon, & Marziani, 2018): the parameters $\text{FWHM H}\beta$ and R_{FeII} constrain the source within the B1, with an occasional excursus in bin B1⁺⁺, in correspondence of the luminosity minimum. We are still waiting for a changing look AGN that transitions from a Pop. B to a Pop. A spectral type following a large increase in luminosity; this phenomenon would provide further positive evidence of the spectral type association with Eddington ratio.⁴

If the BLR radius follows a scaling relation in the form of a power-law with luminosity ($r \propto L^a$, Bentz et al. 2013; Kaspi et al. 2000), under the standard virial assumption, then the line FWHM can be written as a function of the bolometric luminosity, black hole mass M_{BH} , and θ -dependent virial factor:

$$\text{FWHM} \propto f_S(\theta)^{-\frac{1}{2}} \left(\frac{L}{M_{\text{BH}}} \right)^{-\frac{a}{2}} M_{\text{BH}}^{\frac{1-a}{2}} \quad (2)$$

$$\propto f_S(\theta)^{-\frac{1}{2}} L^{\frac{1-a}{2}} \left(\frac{L}{M_{\text{BH}}} \right)^{-\frac{1}{2}}. \quad (3)$$

³According to current accretion disk theory, the accretion rate can be arbitrarily high but the luminosity saturates to a limiting value with $(L/L_{\text{Edd}} \sim 1$ (Mineshige, Kawaguchi, Takeuchi, & Hayashida, 2000).

⁴A change from Pop. B to Pop. A in response to a luminosity increase would disprove the current interpretation of the Eigenvector 1 MS, and is not expected.

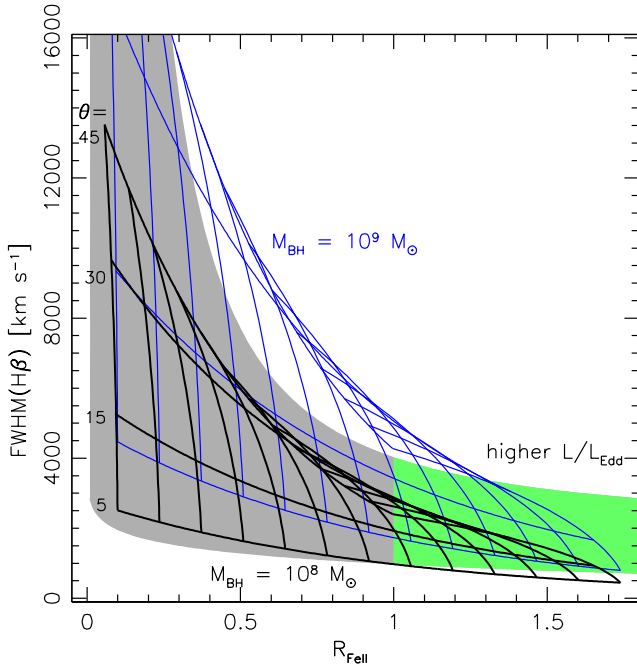


FIGURE 2 The occupation of MS quasars in the plane FWHM $H\beta$ vs R_{FeII} as in Fig 1 with two grids of L/L_{Edd} and θ , for $M_{\text{BH}} = 10^8 M_{\odot}$ (black) and $M_{\text{BH}} = 10^9 M_{\odot}$ (blue). Eddington ratio increase along with R_{FeII} , while viewing angle θ decreases toward the bottom.

If $a = 0.5$, one can easily see that $\text{FWHM} \propto M_{\text{BH}}^{1/4}$ for fixed θ and L/L_{Edd} , implying that the grid is shifted upwards and that the FWHM increases by a factor ~ 1.8 for a ten-fold increase in M_{BH} . Going one step further it is possible to account for the R_{FeII} values in each spectral bin assuming a systematic increase of density, chemical abundances and Eddington ratio from the low R_{FeII} , high FWHM to the high R_{FeII} , low FWHM end of the MS (Panda et al., 2019), keeping a consistency with the r_{BLR} values expected from the scaling $r_{\text{BLR}} - L$ (Bentz et al., 2013), and including the correction derived for highly accreting quasars (Martínez-Aldama et al., 2019).

3 | EXTREME POPULATION B

The extreme Population B involves by definition sources with broad Balmer profiles (a conventional limit could be set at $\approx 10000 \text{ km s}^{-1}$ of at 12000 km s^{-1} to include only the most extreme sources, and very low (often undetectable) R_{FeII} i.e., at variance with Pop. A where the majority of sources have measurable R_{FeII} . A defining feature is the presence of a redward asymmetry, especially prominent in low-ionization lines (Marziani, Zamanov, Sulentic, & Calvani, 2003; Wang et al.,

2017; Wolf et al., 2020). The R_{FeII} parameter is a fundamental one in the definition of the MS, and the FeII flux is expected to be dependent not only on the gas physical conditions but on the chemical abundances as well. It is therefore important to assess the relevance of metallicity Z on the location in optical plane of the MS (Panda et al., 2018; Panda et al., 2019; Punsly, Marziani, Bennert, Nagai, & Gurwell, 2018). A second important result coming from the MS occupation is that, at variance with Pop. A, extreme Pop. B encompasses the largest prevalence of “jetted” sources. It is intriguing that the jetted sources differ from the RQ ones in the distribution of blueshift of high ionization lines, while there is a minor effect of radio-loudness on the low-ionization lines (Richards et al., 2011; Sulentic, Bachev, Marziani, Negrete, & Dultzin, 2007). Extreme Pop. A also includes a significant fraction of powerful radio emitters, but their nature is probably very different from the one of the jetted sources in Pop. B, as discussed in § 4.2.

3.1 | Chemical composition analysis

While the MS emission line trends might be mainly governed by a trend in ionization parameter and density, there are other factors that may play a concomitant role, and whose importance is still debated (see e.g., Temple, Ferland, Rankine, Chatzikos, & Hewett, 2021). One of them is the metal content of the line emitting gas. We considered the active galaxy NGC 1275 (a.k.a. 3C 84 or Perseus A, a radio-loud AGN with an optical spectrum of Pop. B), and analyzed the rest-frame optical and UV spectra to measure the chemical abundance of its BLR gas. A full account of the analysis is provided by Punsly, Marziani, et al. (2018). The source has a very faint BLR compared to the prominent narrow-line region emission but, once this difficulty has been overcome via a careful multi-component nonlinear fit, it was possible to gain constraints on the target line flux ratios: $R_{\text{FeII}} \lesssim 0.3$, $\text{FWHM } H\beta \approx 5000 \text{ km s}^{-1}$ (implying a spectral type B1 in the MS context)⁵, low $[\text{CIV}]\lambda 1549/\text{HeII}\lambda 1640$ and $\text{CIV}\lambda 1549/H\beta$ ratios, high $\text{HeII}\lambda 4686/H\beta$. The fit was carried out using a non-linear, multicomponent, minimum χ^2 approach with the same technique described in several previous papers (e.g., Marziani et al., 2010; Sulentic et al., 2015). We exploit here an empirical advantage of the MS: for most of the bins it is possible to consider composites or even a single object as representative of the spectral type (Marziani et al., 2010), as (the only exception being perhaps A1; Panda et al. 2019) the sources scatter around a well defined average.

Recent analyses utilized photoionization computations that cover a six-dimensional parameter space (spectral energy distribution (SED), ionization parameter, density, column density

⁵The same considerations however apply to extreme Pop. B, considering that those sources show emission line ratios similar to the NGC 1275.

metallicity, micro-turbulence; Panda et al. 2018). Exploration of a parameter subspace in density, ionization parameter U , column density, and metallicity with CLOUDY 17.01 (Ferland et al., 2017) assuming a carefully defined SED on the basis of multifrequency observations (a full description is provided by Punsly, Marziani, et al. 2018) yielded a set of possible solution in agreement with the diagnostic ratios, and with the observed line luminosity: $n_{\text{H}} \sim 10^{10} \text{ cm}^{-3}$, $N_{\text{H}} \sim 10^{23} \text{ cm}^{-2}$, $0.1 Z_{\odot} \lesssim Z \lesssim 1 Z_{\odot}$ (Punsly, Marziani, et al., 2018). These values are consistent with the ones assumed by Panda et al. (2019) for the Pop. B spectral bins.

3.2 | Orientation analysis

Type-1 quasars showing a Fanaroff-Riley II morphology are associated with very low Eddington ratio and moderate θ . Actually the core-to-lobe ratio and the core-to-optical fluxes have been used as an orientation indicator (Wills & Brotherton, 1995; Wills & Browne, 1986). In the MS context, Fanaroff-Riley II quasars and also jetted sources (satisfying the rather strict condition on the radio-to-optical flux $\gtrsim 80$ Padovani, 2017; Sulentic et al., 2003) are constrained within Pop. B, with few core-dominated sources entering the domain of Pop- A (i.e., appearing with $\text{FWHM H}\beta \lesssim 4000 \text{ km s}^{-1}$) because of the almost face-on orientation (Sulentic et al., 2003). Fig. 3 illustrates the appearance of line profiles for two objects of Pop. B with widely different line widths, Arp 102B and the blazar PKS 0438-436. Both objects are fairly well representative of their classes: Arp 102B for double-peaked sources, and PKS 0438-436 for blazars. The middle panel illustrates the displacement expected on the basis of the interpretation scheme outlined in §2.

3.2.1 | Moderate-to-high viewing angles

Sources with widely-separated double peaks attracted a lot of attention in the years 1990s and 2000s. Very broad Population B sources that show a double peaked Balmer line profile have been long since considered as candidate accretion disk profiles (Chen, Halpern, & Filippenko, 1989). They are rare ($\sim 2\%$ in the SDSS; Strateva et al. 2003) and, after discounting the hypothesis of a binary black hole (Halpern & Filippenko, 1988) on the basis of long-term monitoring (Eracleous, Halpern, Gilbert, Newman, & Filippenko, 1997), as well as the possibility of a bipolar outflow (Sulentic, Calvani, Marziani, & Zheng, 1990; Zheng, Sulentic, & Binette, 1990) for lack of evidence, the present consensus is that the profiles are genuinely representative of disk emission, possibly without strict axial symmetry (E. Bon, Jovanović, Marziani, Bon, & Otašević, 2018; Eracleous, Livio, Halpern, & Storchi-Bergmann, 1995). Basically, the radial velocity stability of the

double-peaked structure ruled out alternative models. The prototypical source Arp 102B is relatively bright and luminous ($M_{\text{R}} \approx -25.7$) but nowadays very similar profiles are being discovered in lower luminosity AGN (Bianchi et al., 2019), thanks to the careful subtraction of the host galaxy continuum made possible by the use of integral field spectroscopy. Models of accretion disks are consistent with viewing angle around $30 - 50$ degrees, and show the red wing with redshift amplitude δz consistent with the effect of gravitational and transverse redshift (N. Bon, Bon, Marziani, & Jovanović, 2015; Corbin, 1995; Popovic, Vince, Atanackovic-Vukmanovic, & Kubicela, 1995; Zheng & Sulentic, 1990), i.e.

$$\delta z \approx \frac{3}{2} \frac{r_{\text{g}}}{\tilde{r}_{\text{BLR}}} \quad (4)$$

where r_{g} is the gravitational radius, and \tilde{r}_{BLR} corresponds to innermost radii of the BLR, if the δz measurement is obtained from the line centroid close to the line base (for example, 0.1 or 0.25 of maximum intensity).

3.2.2 | Low viewing angles

The emission line profiles of radio-loud quasars are often characterized by extreme redward asymmetries in the line profiles (Marziani, Sulentic, Dultzin-Hacyan, Calvani, & Moles, 1996; Punsly, 2010). A recent survey of blazar spectra (Punsly, Marziani, Berton, & Kharb, 2020) show consistency with a large contribution from the inner region of an accretion disk to the line profiles, with disk inner radius $\tilde{r}_{\text{BLR}} \lesssim 100 r_{\text{g}}$. In this case, the model profiles constrain the disk viewing angle to be $\theta \lesssim 5$ degrees. The accretion disk emission is favored by the low level of the ionizing continuum: if normalized to the optical flux, the emission is about two order of magnitude lower in the FUV domain with respect to NGC 5548, the prototypical Population B source. The flatness of the emitting region added a second element that helped to detect the effect of orientation, if the blazar profiles are compared to the ones of more inclined sources such as Arp 102B.

The detection of gravitational redshift requires efficient illumination of the inner disk, which may be provided by low luminosity or by particular geometries, for example a warped disk (Jiang et al., 2021). As a corollary, it is unclear whether redshifted line wings in all of Population B can be explained as due to gravitational and transverse redshift. The CIV $\lambda 1549$ shown in Fig. 3 illustrates the point: while the red wing is well reproduced by a disk model, the core and the blue line sides are affected by additional line emission roughly at rest frame, as well as by an outflowing component yielding an excess emission that voids the information from the centroid close to the line base (E. Bon, 2008; E. Bon, Popović, Gavrilović, Mura, & Mediavilla, 2009; E. Bon, Popović, Ilić, & Mediavilla, 2006; Popović, Mediavilla, Bon, & Ilić, 2004).

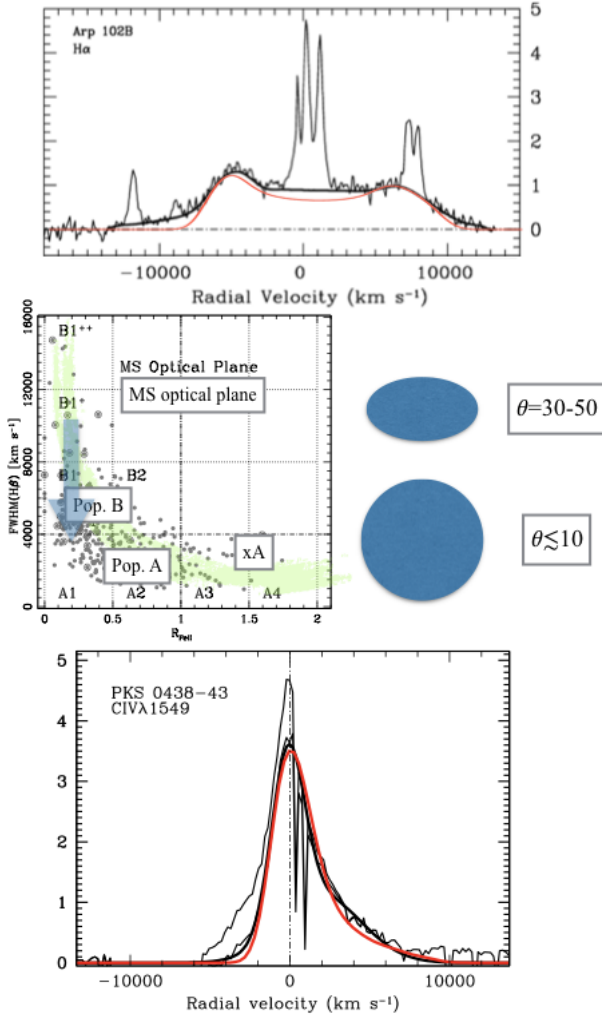


FIGURE 3 Effect of the viewing angle on the line profiles of emission lines for $R_{\text{FeII}} \sim 0$. The top panel shows the H α profile of Arp 102B, in the rest frame, after continuum subtraction and atmospheric absorption correction (Sulentic et al., 1990). The black line shows an empirical fit to the broad emission, while the red one is the relativistic accretion disk model (inner and outer radius $r_{\text{in}} = 350r_g$, $r_{\text{out}} = 1000r_g$, $\theta = 32$). The middle panel is meant to illustrate the effect of a large change in viewing angle θ over the location of a source in the optical plane of the MS at $R_{\text{FeII}} \sim 0$, in accordance with the prediction of an accretion disk seen at different orientation. The CIV profile of the blazar PKS 0438-436 has been analysed by Punsly, Tramacere, et al. (2018). In this case the disk model has been computed for inner and outer radius $r_{\text{in}} = 100r_g$, $r_{\text{out}} \approx 8000r_g$, $\theta = 9$.

4 | EXTREME POPULATION A

The extreme Population A (xA) is made of FeII emitters with $R_{\text{FeII}} \gtrsim 1$ (Marziani & Sulentic, 2014). The CIV λ 1549

is mainly blueshifted (i.e. wind) emission but Balmer and Paschen lines remain predominantly virialized (Martínez-Aldama et al., 2018). The selection criterion $R_{\text{FeII}} \gtrsim 1$ corresponds to an UV selection criterion based on two diagnostic ratios implying strong Aluminium and Silicon lines and weak CIII] λ 1909. At the origin of the interest in xA sources (some of which might be highly super-Eddington accretors, Wang et al. 2014) is the fact that xA population quasars radiate close to an extreme Eddington ratio (Marziani & Sulentic, 2014), and this property may be exploited to define standard “Eddington candles” for cosmology (e.g., Marziani et al., 2021, and references therein).

4.1 | Chemical composition analysis

Emission line ratios in a photoionization context are dependent on the SED of the ionising radiation that is known in turn to depend on Eddington ratio (Ferland, Done, Jin, Landt, & Ward, 2020; Laor, Fiore, Elvis, Wilkes, & McDowell, 1997), and hence on the location along the MS. Arrays of Cloudy 17.02 (Ferland et al., 2017) photoionization simulations were computed covering the U — density parameter plane with a step of 0.25 dex, for 12 values of metallicity covering the range $0.01 Z_{\odot} \leq Z \leq 1000Z_{\odot}$, with a SED appropriate for sources radiating at high Eddington ratio, including a prominent big blue bump. A detailed account of the simulation settings and a systematic presentation of the physical basis of the method and of the results is provided by Marziani, del Olmo, Perea, D’Onofrio, & Panda (2020) and Śniegowska et al. (2021). The simulation results show that diagnostic line ratios CIV λ 1549/HeII λ 1640, AlIII λ 1860/HeII λ 1640, (SiIV+OIV)] λ 1400/HeII λ 1640 are monotonically increasing with Z over a wide range of ionization parameter values, for a fixed SED (Śniegowska et al., 2021). The HeII λ 1640 emission line is expedient because of unchanging He abundance and of simple HeII λ 1640 radiation transfer (collisional excitation is negligible, as the lower transition level is at a high energy above ground $\approx 40\text{eV}$; Marziani, del Olmo, et al. 2020).

In terms of metallicity, xA sources show very homogeneous properties and extreme values of metallicity ($Z \gtrsim 10Z_{\odot}$; $Z \sim 20Z_{\odot}$ seems a typical value). For the low-ionization BLR, ionization parameter, density, and Z are constrained within a relatively narrow range for most xA sources (Śniegowska et al., 2021). Systematic differences in the Z derived from the different ratios may imply over-abundances of Al and Si ($Z(\text{AlIII}/\text{HeII}) \sim 20 - 50Z_{\odot}$) with respect to C, since $Z(\text{CIV}/\text{HeII}) \sim 10Z_{\odot}$ (Garnica et al. 2021, in preparation). The difference persists over a rather wide range in ionization parameter and density, and is most likely due to scaling by

a fixed factor under the assumption that all relative elemental abundances of the BLR are solar. This approach does not take into account that solar relative abundances are most likely inappropriate in the nuclear and circumnuclear regions of AGN.

4.2 | Radio properties

An unexpected finding was a high prevalence of radio-intermediate (with radio-to-optical specific flux in the range 10 — 80) or even radio-loud quasars in xA that can reach very high radio power $P_\nu \lesssim 10^{25} \text{ W Hz}^{-1}$, comparable to the low end of the distribution of jetted sources (Zamfir et al., 2008). Moving along the sequence from spectral type from B1⁺⁺ to A4, the fraction of radio-loud and radio-intermediate peaks at the two extremes.

A possible interpretation is the existence of a population of jetted sources of moderate luminosity, associated with small black hole masses (RL NLSy1s, Komossa et al., 2006). However, the xA radio-intermediate might not follow the same relation between radio power and radio-to-optical flux ratio (Fig. 4, and del Olmo et al. 2021). WISE colors indicate that star formation in the host galaxies can give a significant contribution to the radio power (Caccianiga et al., 2015). Ganci et al. (2019) showed that the xA sources with significantly high radio power obey the correlation between FIR luminosity and radio power expected for star-forming galaxies and radio-quiet quasars (c.f. Bonzini et al., 2015). A radio power $P_\nu \sim 10^{25} \text{ W Hz}^{-1}$ translates into an enormous star-formation rate $\text{SFR} \sim 10^4 M_\odot \text{ yr}^{-1}$, implying that most of the host (and not only the circumnuclear regions) might be experiencing a burst of star formation. This might be unlikely at low redshift, but not at the “cosmic noon.”

4.3 | Orientation effects

The orientation effects on xA sources specifically have been analyzed in several recent papers (Dultzin et al., 2020; Marziani, Bon, et al., 2020; Negrete et al., 2018). xA samples are biased: since they have low line equivalent width (Martínez-Aldama et al., 2018), they are preferentially selected with narrower lines, and narrower lines might imply low inclination. This said, xA sources are accreting at very high rates, implying that their luminosity per unit mass converges toward a limiting value (Wang, Du, Valls-Gabaud, Hu, & Netzer, 2013). This property can be, in principle, used to define “Eddington standard candles,” in which the Eddington ratio, and not the luminosity, has a small scatter around a well-defined value (Marziani & Sulentic, 2014). Since the virial luminosity is derived from the assumption $L/M_{\text{BH}} \sim \text{const}$, lower L is implied by narrower line width, and the FWHM decreases with decreasing amplitude of the viewing angle,

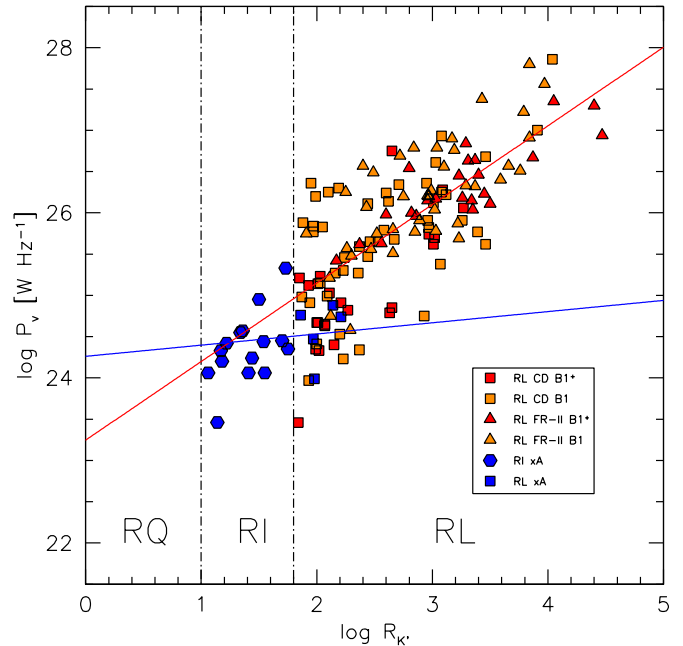


FIGURE 4 Relation between radio power and radio-to-optical flux ratio for the xA sources and for jetted sources of Pop. B spectral types. Squares and triangles: compact and FR-II radio-loud; hexagons: radio-intermediate. Red: spectral type B1⁺, orange: B1; navy blue: xA represented by spectral type A3 and A4, squares for RL, and exagons for radio intermediate (RI). The dot-dashed lines separate the domain of RQ, RI, and RL Pop. B. The blue and red lines are an unweighted lsq fit for the xA sources and for the RL Pop. B objects, respectively.

a relation can be established between viewing angle θ and the difference between the virial luminosity and luminosity derived from concordance cosmology. The resulting distribution covers the range from $0 \lesssim \theta \lesssim 50$, with a maximum at $\theta \approx 20$ (Marziani, Bon, et al., 2020; Negrete et al., 2018), with a relatively small dispersion. At least the xA sources that were analyzed in the previous works are seen predominantly almost face-on.

5 | CONCLUSION

Recent developments strengthen the interpretation of the MS of quasars based on Eddington ratio and orientation. At the Population B extremes, the broad line emitting regions appear as “disk dominated” and the flatness of the emitting region helped detect orientation effects. The MS is not only about spectral parameters; instead, it reflects different evolutionary and environmental situations. In Population B, an estimate of metallicity Z for a fairly typical source suggest solar or

slightly sub-solar metallicity. At the other extreme of the main sequence, extreme of Population A appear to be in highly star forming hosts, very metal rich, possibly with enrichment associated with a circumnuclear Starburst or nuclear accretion modified stars (D’Onofrio & Marziani, 2018). Preliminary attempts to build a Hubble diagram with xA sources are still affected by large dispersion in the distance modulus estimates (Czerny et al., 2021; Dultzin et al., 2020). Large samples (ideally recognized via machine learning, Jankov et al. 2021; Peruzzi et al. 2021 could help) reduce the statistical dispersion. However, the additional complexity related to SED and circumnuclear environment needs to be thoroughly analyzed to safely exploit xA sources as Eddington standard candles.

Author contributions

PM wrote the paper. The other authors contributed in various form to several publications summarized in the text. We thank the reviewer whose suggestion greatly contributed to improve the clarity and completeness of the paper.

Financial disclosure

NB and EB acknowledge the support of Serbian Ministry of Education, Science and Technological Development, through the contract number 451-03-68/2020-14/200002.

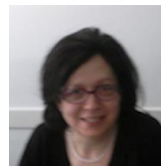
REFERENCES

- Antonucci, R. 1993, *ARA&A*, 31, 473-521. doi:
- Bentz, M. C., Denney, K. D., Grier, C. J. et al. 2013, April, *ApJ*, 767, 149. doi:
- Bianchi, S., Antonucci, R., Capetti, A. et al. 2019, September, *MNRAS*, 488(1), L1-L5. doi:
- Bon, E. 2008, December, *Serbian Astronomical Journal*, 177, 9-13. doi:
- Bon, E., Jovanović, P., Marziani, P., Bon, N., & Otašević, A. 2018, June, *Frontiers in Astronomy and Space Sciences*, 5, 19. doi:
- Bon, E., Popović, L. Č., Gavrilović, N., Mura, G. L., & Mediavilla, E. 2009, December, *MNRAS*, 400, 924-936. doi:
- Bon, E., Popović, L. Č., Ilić, D., & Mediavilla, E. 2006, November, *New A Rev.*, 50(9-10), 716-719. doi:
- Bon, N., Bon, E., & Marziani, P. 2018, January, *Frontiers in Astronomy and Space Sciences*, 5, 3. doi:
- Bon, N., Bon, E., Marziani, P., & Jovanović, P. 2015, December, *Ap&SS*, 360, 7. doi:
- Bon, N., Marziani, P., Bon, E. et al. 2020, March, *A&A*, 635, A151. doi:
- Bonzini, M., Mainieri, V., Padovani, P. et al. 2015, October, *MNRAS*, 453, 1079-1094. doi:
- Boroson, T. A., & Green, R. F. 1992, May, *ApJS*, 80, 109. doi:
- Caccianiga, A., Antón, S., Ballo, L. et al. 2015, August, *MNRAS*, 451(2), 1795-1805. doi:
- Chen, K., Halpern, J. P., & Filippenko, A. V. 1989, April, *ApJ*, 339, 742-751. doi:
- Collin-Souffrin, S., Dyson, J. E., McDowell, J. C., & Perry, J. J. 1988, June, *MNRAS*, 232, 539-550.
- Corbin, M. R. 1995, July, *ApJ*, 447, 496-+. doi:
- Czerny, B., Martínez-Aldama, M. L., Wojtkowska, G. et al. 2021, April, *Acta Physica Polonica A*, 139(4), 389-393. doi:
- del Olmo, A., Marziani, P., Ganci, V., D’Onofrio, M., Bon, E., Bon, N., & Negrete, A. C. 2021, January, *IAU Symposium*, 356, 310-313. doi:
- D’Onofrio, M., & Marziani, P. 2018, September, *Frontiers in Astronomy and Space Sciences*, 5, 31. doi:
- D’Onofrio, M., Marziani, P., & Chiosi, C. 2021, September, *arXiv e-prints*, arXiv:2109.06301.
- Du, P., Wang, J.-M., Hu, C., Ho, L. C., Li, Y.-R., & Bai, J.-M. 2016, February, *ApJ*, 818, L14. doi:
- Dultzin, D., Marziani, P., de Diego, J. A. et al. 2020, January, *Frontiers in Astronomy and Space Sciences*, 6, 80. doi:
- Elvis, M. 2000, December, *ApJ*, 545, 63-76. doi:
- Eracleous, M., Halpern, J. P., Gilbert, A. M., Newman, J. A., & Filippenko, A. V. 1997, November, *ApJ*, 490, 216-+. doi:
- Eracleous, M., Livio, M., Halpern, J. P., & Storchi-Bergmann, T. 1995, January, *ApJ*, 438, 610-622. doi:
- Ferland, G. J., Chatzikos, M., Guzmán, F. et al. 2017, October, *Rev. Mexicana Astron. Astrofis.*, 53, 385-438.
- Ferland, G. J., Done, C., Jin, C., Landt, H., & Ward, M. J. 2020, May, *MNRAS*, 494(4), 5917-5922. doi:
- Fraix-Burnet, D., Marziani, P., D’Onofrio, M., & Dultzin, D. 2017, *Frontiers in Astronomy and Space Sciences*, 4, 1. Retrieved from <http://journal.frontiersin.org/article/10.3389/fspas.2017.00001> doi:
- Ganci, V., Marziani, P., D’Onofrio, M., del Olmo, A., Bon, E., Bon, N., & Negrete, C. A. 2019, October, *A&A*, 630, A110. doi:
- Gaskell, C. M. 1985, April, *ApJ*, 291, 112-116. doi:
- Halpern, J. P., & Filippenko, A. V. 1988, January, *Nature*, 331, 46-48. doi:
- Jankov, I., Ilić, D., & Kovačević, A. 2021, June, *Publications de l’Observatoire Astronomique de Beograd*, 100, 241-246.
- Jiang, B.-W., Marziani, P., Savić, Đ. et al. 2021, August, *MNRAS*. doi:
- Kaspi, S., Smith, P. S., Netzer, H., Maoz, D., Jannuzi, B. T., & Giveon, U. 2000, April, *ApJ*, 533, 631-649. doi:
- Komossa, S., Voges, W., Xu, D. et al. 2006, August, *AJ*, 132, 531-545. doi:
- Laor, A., Fiore, F., Elvis, M., Wilkes, B. J., & McDowell, J. C. 1997, March, *ApJ*, 477, 93-+. doi:
- Marin, F. 2016, August, *MNRAS*, 460(4), 3679-3705. doi:
- Marinello, A. O. M., Rodríguez-Ardila, A., García-Rissmann, A., Sigut, T. A. A., & Pradhan, A. K. 2016, February, *ApJ*, 820(2), 116.
- Martínez-Aldama, M. L., Czerny, B., Kawka, D., Karas, V., Panda, S., Zajaček, M., & Życki, P. T. 2019, October, *ApJ*, 883(2), 170. doi:
- Martínez-Aldama, M. L., del Olmo, A., Marziani, P. et al. 2018, November, *A&A*, 618, A179. doi:
- Marziani, P., Bon, E., Bon, N. et al. 2020, January, *Contributions of the Astronomical Observatory Skalnaté Pleso*, 50(1), 244-256. doi:
- Marziani, P., del Olmo, A., D’Onofrio, M. et al. 2018, April, Narrow-line Seyfert 1s: what is wrong in a name? Revisiting narrow-line Seyfert 1 galaxies and their place in the Universe. 9-13 April 2018. Padova Botanical Garden, Italy. Online at https://pos.sissa.it/cgi-bin/reader/conf.cgi?confid=328, id.2 Vol. PoS(NLS1-2018), p. 002. SISSA/ISAS.

- Marziani, P., del Olmo, A., Perea, J., D'Onofrio, M., & Panda, S. 2020, December, *Atoms*, 8(4), 94. doi:
- Marziani, P., Dultzin, D., del Olmo, A. et al. 2021, January, *IAU Symposium*, 356, 66-71. doi:
- Marziani, P., Dultzin, D., Sulentic, J. W. et al. 2018, March, *Frontiers in Astronomy and Space Sciences*, 5, 6. doi:
- Marziani, P., & Sulentic, J. W. 2014, August, *MNRAS*, 442, 1211-1229. doi:
- Marziani, P., Sulentic, J. W., Dultzin-Hacyan, D., Calvani, M., & Moles, M. 1996, May, *ApJS*, 104, 37-+. doi:
- Marziani, P., Sulentic, J. W., Negrete, C. A., Dultzin, D., D'Onofrio, M., Del Olmo, A., & Martínez-Aldama, M. L. 2014, October, *The Astronomical Review*, 9, 6-25.
- Marziani, P., Sulentic, J. W., Negrete, C. A., Dultzin, D., Zamfir, S., & Bachev, R. 2010, December, *MNRAS*, 409, 1033-1048. doi:
- Marziani, P., Sulentic, J. W., Plauchu-Frayn, I., & del Olmo, A. 2013, May, *AAp*, 555, 89, 16pp.
- Marziani, P., Sulentic, J. W., Zwitter, T., Dultzin-Hacyan, D., & Calvani, M. 2001, September, *ApJ*, 558, 553-560. doi:
- Marziani, P., Zamanov, R. K., Sulentic, J. W., & Calvani, M. 2003, November, *MNRAS*, 345, 1133-1144. doi:
- Mineshige, S., Kawaguchi, T., Takeuchi, M., & Hayashida, K. 2000, June, *PASJ*, 52, 499-508.
- Negrete, C. A., Dultzin, D., Marziani, P. et al. 2018, December, *A&A*, 620, A118. doi:
- Padovani, P. 2017, November, *Frontiers in Astronomy and Space Sciences*, 4, 35. doi:
- Panda, S., Czerny, B., Adhikari, T. P., Hryniewicz, K., Wildy, C., Kuraszkiwicz, J., & Śniegowska, M. 2018, oct, *The Astrophysical Journal*, 866(2), 115. Retrieved from <https://doi.org/10.3847/2F1538-4357/2Faae209> doi:
- Panda, S., Marziani, P., & Czerny, B. 2019, September, *ApJ*, 882(2), 79. doi:
- Peruzzi, T., Pasquato, M., Ciroi, S., Berton, M., Marziani, P., & Nardini, E. 2021, August, *A&A*, 652, A19. doi:
- Popović, L. Č., Mediavilla, E., Bon, E., & Ilić, D. 2004, September, *A&A*, 423, 909-918. doi:
- Popovic, L. C., Vince, I., Atanackovic-Vukmanovic, O., & Kubicela, A. 1995, January, *A&A*, 293, 309-314.
- Punsly, B. 2010, April, *ApJ*, 713, 232-238. doi:
- Punsly, B., Marziani, P., Bennert, V. N., Nagai, H., & Gurwell, M. A. 2018, December, *ApJ*, 869, 143. doi:
- Punsly, B., Marziani, P., Berton, M., & Kharb, P. 2020, November, *ApJ*, 903(1), 44. doi:
- Punsly, B., Tramacere, A., Kharb, P., & Marziani, P. 2018, December, *ApJ*, 869(2), 174. doi:
- Richards, G. T., Kruczek, N. E., Gallagher, S. C. et al. 2011, May, *AJ*, 141, 167-+. doi:
- Shen, Y., & Ho, L. C. 2014, September, *Nature*, 513, 210-213. doi:
- Śniegowska, M., Marziani, P., Czerny, B., Panda, S., Martínez-Aldama, M. L., del Olmo, A., & D'Onofrio, M. 2021, April, *ApJ*, 910(2), 115. doi:
- Strateva, I. V., Strauss, M. A., Hao, L. et al. 2003, October, *AJ*, 126, 1720-1749. doi:
- Sulentic, J. W., Bachev, R., Marziani, P., Negrete, C. A., & Dultzin, D. 2007, September, *ApJ*, 666(2), 757-777. doi:
- Sulentic, J. W., Calvani, M., Marziani, P., & Zheng, W. 1990, May, *ApJ*, 355, L15. doi:
- Sulentic, J. W., Martínez-Carballo, M. A., Marziani, P., del Olmo, A., Stirpe, G. M., Zamfir, S., & Plauchu-Frayn, I. 2015, June, *MNRAS*, 450, 1916-1925. doi:
- Sulentic, J. W., Marziani, P., & Dultzin-Hacyan, D. 2000, *ARA&A*, 38, 521-571. doi:
- Sulentic, J. W., Marziani, P., Zamanov, R., Bachev, R., Calvani, M., & Dultzin-Hacyan, D. 2002, February, *ApJL*, 566, L71-L75. doi:
- Sulentic, J. W., Marziani, P., Zwitter, T., Dultzin-Hacyan, D., & Calvani, M. 2000, December, *ApJL*, 545, L15-L18. doi:
- Sulentic, J. W., Zamfir, S., Marziani, P., Bachev, R., Calvani, M., & Dultzin-Hacyan, D. 2003, November, *ApJL*, 597, L17-L20. doi:
- Sun, J., & Shen, Y. 2015, May, *ApJ*, 804, L15. doi:
- Temple, M. J., Ferland, G. J., Rankine, A. L., Chatzikos, M., & Hewett, P. C. 2021, August, *MNRAS*, 505(3), 3247-3259. doi:
- Urry, C. M., & Padovani, P. 1995, September, *PASP*, 107, 803. doi:
- Wang, J.-M., Du, P., Brotherton, M. S. et al. 2017, October, *Nature Astronomy*, 1, 775-783. doi:
- Wang, J.-M., Du, P., Hu, C. et al. 2014, October, *ApJ*, 793(2), 108. doi:
- Wang, J.-M., Du, P., Valls-Gabaud, D., Hu, C., & Netzer, H. 2013, February, *Physical Review Letters*, 110(8), 081301. doi:
- Wills, B. J., & Brotherton, M. S. 1995, August, *ApJ*, 448, L81. doi:
- Wills, B. J., & Browne, I. W. A. 1986, March, *ApJ*, 302, 56-63. doi:
- Wolf, J., Salvato, M., Coffey, D. et al. 2020, March, *MNRAS*, 492(3), 3580-3601. doi:
- Zamfir, S., Sulentic, J. W., & Marziani, P. 2008, June, *MNRAS*, 387, 856-870. doi:
- Zamfir, S., Sulentic, J. W., Marziani, P., & Dultzin, D. 2010, February, *MNRAS*, 403, 1759. doi:
- Zheng, W., & Sulentic, J. W. 1990, February, *ApJ*, 350, 512. doi:
- Zheng, W., Sulentic, J. W., & Binette, L. 1990, December, *ApJ*, 365, 115-118. doi:



AUTHOR BIOGRAPHY



Paola Marziani is an astronomer with the National Institute of Astrophysics (INAF), based at the Padua Astronomical Observatory in Italy.

